Fluctuation-induced forces in critical fluids

1999 J. Phys.: Condens. Matter 11 R391

(http://iopscience.iop.org/0953-8984/11/37/201)

J. Phys.: Condens. Matter **11** (1999) R391–R412. Printed in the UK PII: S0953-8984(99)97485-4

REVIEW ARTICLE

Fluctuation-induced forces in critical fluids

M Krech

Institut für Theoretische Physik, RWTH Aachen, 52056 Aachen, Germany

Received 25 May 1999

Abstract. The current knowledge about fluctuation-induced long-ranged forces is summarized. Reference is made in particular to fluids near critical points, for which some new insight has been obtained recently. Where appropriate, results of analytic theory are compared with computer simulations and experiments.

1. Introduction

Forces between particles are governed by fields which themselves can be considered as composed of particles mediating the interaction by continuous exchange processes. Most prominent in the macroscopic world are electromagnetic fields and gravitational fields. For simplicity we specialize to electromagnetic forces here, but the line of argument sketched out in the following is valid in general. Macroscopic bodies exert electromagnetic forces on one another whenever they are charged, but if they are neutral all electromagnetic forces apparently vanish. Casimir [1] was the first to realize that this is not quite correct, because the electromagnetic field is fluctuating. These fluctuations may be due to quantum fluctuations at zero temperature in vacuum or due to thermal fluctuations in a cavity which is in contact with a heat bath. In any case the fluctuation spectrum, i.e., the energies which are associated with the eigenmodes of the system and the form of the eigenmodes themselves are manifestly influenced by the *geometry* of the system. The geometry is given by an arrangement of surfaces which impose boundary conditions on the fluctuating field and thus determine its mode spectrum. The free energy, which contains all information about the thermodynamic properties of the system, is essentially given by a sum over all modes and therefore the free energy will become geometry dependent. If, for example, two uncharged metallic bodies are placed at a certain distance in vacuum the free energy of the configuration depends on the shape of the bodies and the distance between them. Therefore, there will be an *effective force* acting between the bodies, which is given by the derivative of the free energy with respect to their distance. Note that this force is a direct consequence of the influence of the bodies on the electromagnetic fluctuation spectrum. Apart from the macroscopic length scales set by the geometry there are no other length scales in the system which limit the maximum wavelength of the fluctuations and therefore the force is governed by powers of the imposed length scales and scaling functions of their ratios, i.e., the resulting force is *long ranged*. Due to the history of their discovery [1] these forces are now known as Casimir forces and the influence of boundaries on the functional form of the free energy is known as the *Casimir effect*. It should also be noted that the presence of additional bodies in the above set-up modifies the force between any two of them, i.e., it is not possible to express the Casimir effect as a sum of two-body contributions only.

0953-8984/99/370391+22$30.00

1.1. A classic example

There is a vast body of literature on the various aspects of the Casimir effect in electromagnetism which are beyond the scope of this article. For a summary we refer the reader to review articles dedicated to these subjects [2] and for a recent survey in a more general context we refer the reader to chapter 3 of reference [3]. However, for the understanding of the mechanism and the interpretation of the results it is instructive to demonstrate some of the fundamental physical concepts by a simple example, which we call *classic* here for its historic meaning.

Let us assume that we have two parallel perfectly conducting plates placed at a distance L in vacuum. We further assume that the plates have an infinite lateral extension so that we consider the thermodynamic limit with respect to the surface area $\mathcal{A}$ of the plates and only discuss the free energy $\mathcal{F}$ per unit area, i.e., we calculate $F = \lim_{\mathcal{A}\to\infty} \mathcal{F}/\mathcal{A}$. Note that L is the only macroscopic length scale in the problem. The mode spectrum of the electromagnetic field in this parallel-plate geometry is particularly simple. In three dimensions the wave vector $\boldsymbol{q} = (\boldsymbol{p}, k_n)$ consists of a lateral component $\boldsymbol{p} = (p_x, p_y)$ which is unconstrained by the geometry and a discrete perpendicular component $k_n = n\pi/L$ for $n = 1, 2, 3, \ldots$ due to the condition that the electric field vector at each of the metallic surfaces must be aligned with the surface normal. A single mode is then characterized by $\boldsymbol{p}$ and n, and its energy level spacing is given by

$$\varepsilon_{\boldsymbol{p},n} = \hbar c\sqrt{\boldsymbol{p}^2 + (n\pi/L)^2}. \tag{1.1}$$

The energy content $E_{\boldsymbol{p},n}$ of a particular mode is given by its occupation number $m_{\boldsymbol{p},n} = 0, 1, 2, \ldots$ in the form $E_{\boldsymbol{p},n} = \varepsilon_{\boldsymbol{p},n}(m_{\boldsymbol{p},n} + \frac{1}{2})$. The free energy per unit area is then given by (see also reference [4] for a recent reconsideration of the Casimir effect at general temperature)

$$F = \int^{\Lambda} \frac{\mathrm{d}^2 p}{(2\pi)^2} \sum_{n=1}^{N} \varepsilon_{\boldsymbol{p},n} + 2k_B T \int^{\Lambda} \frac{\mathrm{d}^2 p}{(2\pi)^2} \sum_{n=1}^{N} \ln\left[1 - \exp(-\varepsilon_{\boldsymbol{p},n}/(k_B T))\right] \tag{1.2}$$

where k_B and T denote the Boltzmann constant and the temperature, respectively. An additional factor of two coming from the summation over the polarizations has already been included in equation (1.2). The integration over $\boldsymbol{p}$ is carried out to an ultraviolet cut-off Λ and the sum is truncated at some maximum mode number N. The ultraviolet cut-off parameter Λ is typically determined by the radius of the first Brillouin zone of the plate material. If a is the lattice constant of the material we identify $\Lambda = \pi/a$. The maximum mode number N can be written as $N = L/b$, where b is also a microscopic length scale (see below).

For $T = 0$ only the first term in equation (1.2) remains and this is the first example studied by Casimir [1]. Here, we will discuss the high-temperature limit $k_B T \gg \hbar c\Lambda$, because this allows us to illustrate some aspects of the calculations involved within continuum models like, e.g., the Ginzburg–Landau model on a rather elementary level. For the more general case of layered dielectrics at finite temperature (dispersion forces) we refer the reader to the classical literature [5, 6] and to reference [2]. To leading order in $\hbar c\Lambda/(k_B T)$ we obtain

$$F = 2k_B T \int^{\Lambda} \frac{\mathrm{d}^2 p}{(2\pi)^2} \sum_{n=1}^{N} \ln \frac{\varepsilon_{\boldsymbol{p},n}}{k_B T}. \tag{1.3}$$

Note that the integral and the summation in equation (1.3) are only meaningful for finite cut-off parameters Λ and N. However, we only need the final result in the limits $\Lambda L \gg 1$ and $N \gg 1$. For simplicity we identify $k_B T \sim \hbar c\pi/b$ to the order of magnitude which implies $\Lambda L \ll N$, i.e., $b \ll a$. The integral in equation (1.3) is elementary and the resulting terms

can be arranged as

$$F = \frac{k_B T}{4\pi}\Lambda^2 \sum_{n=1}^{N}\left\{2\ln\left(\frac{\hbar c}{k_B T}\frac{n\pi}{L}\right) + \ln\left(1+\left(\frac{\Lambda L}{n\pi}\right)^2\right) + \left(\frac{n\pi}{\Lambda L}\right)^2\left[\ln\left(1+\left(\frac{\Lambda L}{n\pi}\right)^2\right) - \left(\frac{\Lambda L}{n\pi}\right)^2\right]\right\}. \tag{1.4}$$

The sum over the terms in the second line of equation (1.4) converges, so we can immediately perform the limit $N \to \infty$ here. We obtain

$$F = \frac{k_B T}{4\pi}\Lambda^2\left\{2\ln N! + 2N\ln\left(\frac{\hbar c}{k_B T}\frac{\pi}{L}\right) + \int_0^1 \ln\frac{\sinh\left(\Lambda L\sqrt{x}\right)}{\Lambda L\sqrt{x}}\,\mathrm{d}x\right\} \tag{1.5}$$

where terms which *vanish* in the limit $N \to \infty$ have already been dropped. In order to evaluate equation (1.5) further for large N and ΛL, we employ Stirling's formula and the series expansion of the logarithm. With $\Lambda = \pi/a$ and $N = L/b$ we obtain the final result

$$F = L\frac{\pi k_B T}{2a^2 b}\left[\ln\left(\frac{\hbar c}{k_B T}\frac{\pi}{b}\right) - 1 + \frac{\pi b}{3a}\right] + \frac{\pi k_B T}{8a^2}\left[2\ln\left(\frac{a}{b}\right) + 1\right] - \frac{k_B T}{L^2}\frac{\zeta(3)}{8\pi} + \cdots \tag{1.6}$$

where $\zeta(3) \simeq 1.202$ is a special value of the Riemann zeta function and the dots indicate contributions which are exponentially small in ΛL. All terms which vanish in the limit $N \to \infty$ ($b \to 0$) have consistently been dropped.

The decomposition of the free energy per unit area given by equation (1.6) is a special case of the general decomposition

$$F = LF_b + F_{s,\mathrm{a}} + F_{s,\mathrm{b}} + \delta F_{\mathrm{ab}} \tag{1.7}$$

for a film with two surfaces of type a and b. The leading contribution to F is proportional to L and it corresponds to the *bulk* contribution of the free energy. In our example it is given by the radiation pressure F_b between the plates. The second contribution to equation (1.6) is independent of L and it therefore corresponds to the sum of the surface free energies or *surface tensions* $F_{s,\mathrm{a}} + F_{s,\mathrm{b}}$, where a = b in the above example. The third contribution varies as L^{-2} and it corresponds to the fluctuation-induced long-ranged *Casimir interaction* between the plates, which is the most prominent contribution to the *finite-size* part δF_{ab} of the free energy in our example. Note that the Casimir contribution is *independent* of the microscopic cut-off parameters a and b. Its absolute strength at a given distance L and temperature T is governed by the numerical constant $\Delta = -\zeta(3)/(8\pi) \simeq -0.0478$ which is usually called the *Casimir amplitude*. The Casimir amplitude is negative here, so the Casimir force between the plates is *attractive*. The Casimir interaction can be obtained in very elegant ways known as zeta-function regularization, algebraic cut-off, or exponential cut-off schemes [7]. Their equivalence with respect to the cut-off-independent Casimir interaction has been explicitly shown for the example presented here [8]. For further details see also reference [9].

1.2. Critical phenomena and correlated fluids

The above example for the Casimir effect appears to be very specific at first sight, but the functional form of the free energy given by equations (1.3) and (1.6) is far more general than it seems. In fact, the underlying mechanism which leads to fluctuation-induced long-ranged forces only requires a fluctuating field with geometric restrictions and a macroscopic length scale L imposed by the geometry as the only limiting factor for the wavelength of the fluctuations. Any system which is at a *critical point* also meets this requirement. The fluctuating field in this case is given by the order parameter, and each of the individual

contributions to the free energy as given by equation (1.7) is a sum of a *regular* part and *singular* part which contains the critical behaviour of the system. Right *at* the critical point the correlation length ξ is infinite, so the distance L between the system boundaries provides the only macroscopic length scale as required for the occurrence of long-ranged fluctuation-induced forces. Above the critical point the correlation length is finite and therefore the ratio ξ/L governs the range of these forces. The existence of Casimir forces in critical systems was anticipated by Fisher and de Gennes [10] in the framework of the so-called distant-wall corrections to critical profiles, where in many cases the Casimir amplitudes govern the leading distant-wall correction term to the profile in the vicinity of one of the system boundaries. For details and an extended list of further references the reader is referred to chapter 4 of reference [3] and to reference [11].

It is important to realize that the Casimir amplitudes Δ and the associated scaling functions $\theta(L/\xi)$ that take the place of these amplitudes for *finite* L/ξ (see reference [3] and section 2) are *universal*, i.e., they do not depend on microscopic details of the system under consideration. Note, however, that the precise form of the scaling functions θ depends on the *definition* of the correlation length ξ. For systems with surfaces the concept of universality classes raises the question of whether there is *surface* critical behaviour and to what extent it is governed by *universal surface critical exponents*. During the 1980s this question was answered in favour of the general ideas of critical behaviour and universality, i.e., microscopic surface properties are indeed unimportant. One only has to specify the type of *boundary condition* which the surface imposes on the order parameter. In this respect there are only three fundamentally different *surface universality classes* [12]. In particular, the surface may enhance the order parameter with the result that the system undergoes a second-order phase transition in the presence of an already *ordered* surface (extraordinary transition, E). The surface may also suppress the order parameter with the result that the system undergoes a second-order phase transition in the presence of a *disordered* surface (ordinary transition, O). Finally, the surface and the bulk may order at the *same* temperature (special transition, SB), so the critical point of the system is in fact a *multicritical* point. If the spatial dimensionality d of the system is high enough there are two options for the occurrence of surface order above the bulk critical temperature $T_{c,b}$. The surface may order *spontaneously* at a certain critical temperature $T_{c,s} > T_{c,b}$ *or* the surface may be ordered *externally* by the presence of a *surface field*. The bulk transition in the presence of an externally ordered surface is called the *normal* transition. However, it has been shown recently by rigorous arguments that the normal and the extraordinary transitions only differ by corrections to scaling, so both belong to the extraordinary surface universality class [13]. Surface critical behaviour has already been extensively reviewed [12] (see also chapter 2 of reference [3] for a short summary), so we refrain from giving further details here.

The distinction between the surface universality classes is vital for the Casimir forces, because the Casimir amplitudes Δ and the scaling functions θ depend on them. The simplest boundary conditions apart from periodic ones are *Dirichlet* boundary conditions which suppress the order parameter to zero at the surface. A system with these boundary conditions provides a representation of the ordinary surface universality class. The first systematic field-theoretic calculation of a Casimir amplitude was done by Symanzik [14] for this case. Starting from equation (1.3) the above example essentially reproduces all necessary steps for such a calculation at the one-loop level (Gaussian theory). In general, concepts of the field-theoretic renormalization group are required which cannot be described here. The application of field theory to the critical behaviour of finite systems is a field of ongoing research [15] which has recently furnished unexpected results concerning the occurrence of *nonuniversal* critical finite-size behaviour above the upper critical dimension [16]. For reviews about the general concept of critical finite-size scaling the reader is referred to reference [17].

Above the critical temperature the range of the Casimir force is always limited by the correlation length, but below the critical temperature the situation may be different. In Ising-like systems the correlation length is also finite below $T_{c,b}$ and therefore the Casimir forces have a finite range. If the system has a continuous symmetry, however, *Goldstone modes* cause correlation functions of the order parameter to remain long ranged below $T_{c,b}$. The most prominent examples are XY and Heisenberg ferromagnets which possess an O(N) symmetry with $N = 2$ and $N = 3$, respectively, in contrast to the Ising ferromagnet ($N = 1$). In other words, the correlation length of continuous ferromagnets remains infinite below $T_{c,b}$ and therefore Goldstone modes also give rise to fluctuation-induced long-ranged forces between system boundaries. Fluids with this property are sometimes called *correlated fluids*. The most important examples with respect to experimental realizations are liquid ^{4}He below the superfluid–normal transition [18] and nematic liquid crystals in the nematically ordered phase [19], where fluctuations of the nematic director are responsible for the long-ranged nature of the Casimir force. Near the phase transition to the isotropic phase, fluctuations of the degree of nematic order and the degree of biaxiality generate *short-ranged* corrections to the Casimir force [20].

In summary, we have mentioned three options for the occurrence of fluctuation-induced long-ranged forces: the presence of long-ranged interactions (e.g., electromagnetism; see section 1.1), the presence of critical fluctuations, and the presence of Goldstone modes. In the following overview we will only consider the second option, i.e., systems in the vicinity of critical points. In particular, recent progress in the theoretical understanding of critical Casimir forces for all surface universality classes and especially for curved geometries will be presented. Special attention is also paid to the comparison of Casimir amplitudes and corresponding scaling functions with computer simulations and experiments, which are still in progress at this time. Due to the limited scope of this article other interesting developments in related areas will not be described in any detail and an apology is made in advance to all authors whose work is not explicitly mentioned here. The remainder of this article is organized according to the three main approaches to critical Casimir forces, namely analytic theory, computer simulation, and experiments.

2. Analytic theory

The analytic theory of the Casimir effect in critical systems is based on the concept of finite-size scaling [3, 17]. Exact solutions of model systems in statistical mechanics give only limited access to the finite-size scaling functions, because they are mainly restricted to two-dimensional systems. In $d \geqslant 3$ dimensions only the spherical model can be analysed in a rigorous fashion [21] which has recently been done with special regard to the film geometry in $d = 3$ dimensions [22, 23]. Despite their limitations exact solutions provide valuable insight into the structure of the scaling functions and sometimes the results for $d = 2$ can be used to improve estimates obtained by approximative methods for $d = 3$ (see section 3 of reference [3] and below).

The concept of finite-size scaling is a natural extension of the principle of *scale invariance* to critical systems with geometric constraints on macroscopic length scales. The principle of scale invariance itself may be viewed as a special case of the more general principle of *conformal invariance* (see section 3 of reference [3] and reference [24]). Conformal invariance implies the equivalence of systems with boundaries at $T = T_{c,b}$ if these systems can be mapped onto one another by a conformal transformation. The principle of conformal invariance holds in any dimension, but it is particularly powerful for $d = 2$ due to the exceptionally large number of conformal mappings in this case (large conformal group; see reference [24]). Note that scale

transformations are just very special conformal mappings. In the framework of conformal field theory the *stress tensor* plays a key role [24, 25]. Here we only mention that the thermal average of the stress tensor yields the local Casimir force in a critical system and therefore the stress tensor provides a very important tool in the analytic theory of the Casimir effect. In fact, most of the Casimir amplitudes for $d = 2$ have been obtained from conformal field theory rather than exact solutions (see section 3 of reference [3] and reference [24]).

Many of the experimentally relevant results have been obtained from a field-theoretic analysis of the well-known Ginzburg–Landau Hamiltonian $\mathcal{H}$ with geometric constraints which can be decomposed according to $\mathcal{H} = \mathcal{H}_b + \mathcal{H}_s + \mathcal{H}_e$. The bulk contribution $\mathcal{H}_b$ is given by

$$\mathcal{H}_b = \int_V \mathrm{d}^d x \left[\frac{1}{2}(\boldsymbol{\nabla}\cdot\boldsymbol{\Phi})^2 + \frac{\tau}{2}\Phi^2 + \frac{u}{4!}(\Phi^2)^2 - \boldsymbol{H}\cdot\boldsymbol{\Phi}\right] \tag{2.1}$$

for systems characterized by an N-component order parameter $\boldsymbol{\Phi} = (\phi_1, \ldots, \phi_N)$ confined to a volume V, where $N = 1, 2, 3$ characterize the Ising, XY, and Heisenberg universality class, respectively. The parameters τ and $\boldsymbol{H}$ correspond to the bare reduced temperature and external field. The physical (renormalized) reduced temperature and external field will be denoted by t and h in the following. The surface contribution $\mathcal{H}_s$ can be written as

$$\mathcal{H}_s = \int_S \mathrm{d}^{d-1} x \left[\frac{c}{2}\Phi^2 - \boldsymbol{H}_1\cdot\boldsymbol{\Phi}\right] \tag{2.2}$$

where c and $\boldsymbol{H}_1$ correspond to the surface enhancement and the surface field, respectively [12]. Note that the surface S may consist of several disjoint parts. The last contribution $\mathcal{H}_e$ contains edge and curvature contributions to the Hamiltonian $\mathcal{H}$ which were first considered in reference [14] within the framework of the renormalization group. For experiments the ordinary transition ($c = \infty$) and the extraordinary transition (e.g., $c = -\infty$; see also reference [13]) are the most important cases. Neither $\mathcal{H}_s$ nor $\mathcal{H}_e$ needs to be considered here in any detail, because their effect is completely contained in the boundary conditions for the order parameter $\boldsymbol{\Phi}$. We will therefore restrict the following discussion to the ordinary and the extraordinary surface universality class and to periodic boundary conditions.

2.1. The spherical model

The spherical model can be considered as the $N \to \infty$ limit of O(N)-symmetric classical spin models and it can also be expressed as the $N \to \infty$ limit of equations (2.1) and (2.2). We only summarize the most recent results here; for a brief overview the reader is referred to section 2.2 of reference [3] and to reference [21]. In the presence of an external field h and for sufficiently small values of the reduced temperature $t = (T - T_{c,b})/T_{c,b}$ the *singular* contribution δf_{ab} to the finite-size part δF_{ab} of the free energy per unit area in a film geometry (see equation (1.7)) in d dimensions can be cast into the scaling form [22]

$$\delta f_{\mathrm{ab}}(t, h, L) = k_B T_{c,b} L^{-(d-1)} \theta_{\mathrm{ab}}(t L^{1/\nu}, h L^{\beta\delta/\nu}) \tag{2.3}$$

near the critical point given by $t = 0$ and $h = 0$, where ab indicates the combination of surface universality classes at the two surfaces. The critical exponents ν and β characterize the temperature dependence of the correlation length $\xi \sim t^{-\nu}$, $t > 0$, and the order parameter (spontaneous magnetization) $m \sim (-t)^{\beta}$, $t < 0$, for $h = 0$, respectively. The exponent δ characterizes the functional dependence of the magnetization $m \sim |h|^{1/\delta}$ on the external field h for $t = 0$. The form of the scaling arguments in equation (2.3) is imposed by the principle of scale invariance. They can be obtained by observing that L/ξ is equivalent to the first scaling argument and L/ξ_h, where $\xi_h \sim h^{-\nu/(\beta\delta)}$ is the correlation length for finite field h at $t = 0$, is equivalent to the second scaling argument. For nearest-neighbour interactions for $d = 3$ the

critical exponents ν, β, and δ of the spherical model are given by $\nu = 1$, $\beta = 1/2$, and $\delta = 5$. The special value $\Delta_{ab} \equiv \theta_{ab}(0, 0)$ of the scaling function is the Casimir amplitude. In units of $k_B T_{c,b}$ the Casimir force

$$\mathcal{K}_{ab} \equiv -\frac{\partial}{\partial L}\delta f_{ab}$$

is characterized by the corresponding scaling form

$$\mathcal{K}_{ab}(t, h, L) = L^{-d} K_{ab}(tL^{1/\nu}, hL^{\beta\delta/\nu}) \tag{2.4}$$

where the scaling function K_{ab} is given by

$$K_{ab}(x, y) = (d-1)\theta_{ab}(x, y) - \frac{1}{\nu}x\,\frac{\partial}{\partial x}\theta_{ab}(x, y) - \frac{\beta\delta}{\nu}y\,\frac{\partial}{\partial y}\theta_{ab}(x, y). \tag{2.5}$$

The universal scaling functions θ_{ab} and K_{ab} have been investigated recently for periodic boundary conditions ab $=$ *per* [22, 23]. For $h = 0$ the scaling functions $\theta_{per}(x, 0)$ and $K_{per}(x, 0)$ are both negative and increase monotonically with x, i.e., unlike the scaling functions in Ising-like systems they do not have a minimum in the vicinity of $T = T_{c,b}$ ($x = 0$) [22]. For $x \to +\infty$, both scaling functions decay to zero exponentially, whereas for $x \to -\infty$, $K_{per}(x, 0) \to -\zeta(3)/\pi \simeq -0.382$. This behaviour is due to the presence of *Goldstone modes* in the spherical model below $T_{c,b}$. For finite values of h ($y \neq 0$) the scaling functions $\theta_{per}(x, y)$ and $K_{per}(x, y)$ again decay exponentially as $L \to \infty$ [22]. Moreover, both scaling functions also decay exponentially for $y \to \infty$ at $x = 0$. The Casimir amplitude

$$\Delta_{per} = \theta_{per}(0, 0) = -\frac{2\zeta(3)}{5\pi} = -0.153\,05\ldots \tag{2.6}$$

can be obtained exactly [23] and numerically it is very close the best available estimates for the Ising model for $d = 3$ (see table 1 in section 3). It has also been shown rigorously that the scaling function $\theta_{per}(x, y)$ is a monotonically increasing function of each of its arguments as long as the temperature T is in the vicinity of $T_{c,b}$ [23]. However, the *hypothesis* that this statement is true for *any* nearest-neighbour O(N)-symmetric spin model for $N \geqslant 2$ [23] cannot be substantiated so far (see below).

2.2. The Ginzburg–Landau model

2.2.1. Film geometry. The film geometry has also been reinvestigated for the Ginzburg–Landau model for the case of the extraordinary surface universality class [26], which is of particular interest for experiments with critical binary liquid mixtures. The scaling functions $K_{ab}(x, 0)$ in zero external field have been determined within mean-field theory for infinitely strong surface fields $\boldsymbol{h}_1$ and $\boldsymbol{h}_2$ which enclose an arbitrary angle α between $\alpha = 0$ (parallel surface fields) and $\alpha = \pi$ (antiparallel surface fields). For Ising-like systems only $\alpha = 0$ and $\alpha = \pi$ can be realized and we refer to these cases as ab $= ++$ and ab $= +-$. The Casimir amplitude is negative for $\alpha = 0$ and positive for $\alpha = \pi$; it changes sign at $\alpha = \pi/3$ [26]. Accordingly, the scaling function $K_{++}(x, 0)$ is negative and the scaling function $K_{+-}(x, 0)$ is positive for all x within mean-field theory, but it seems very likely that this is also true beyond mean-field theory. The functional form of $K_{++}(x, 0)$ and $K_{+-}(x, 0)$ is illustrated in figure 1, where the normalization of reference [26] has been used. Note that both scaling functions take their extremal values at nonzero x, which makes them qualitatively very similar to the corresponding scaling functions for an Ising strip for $d = 2$, which can be solved exactly [27].

The one-loop corrections to the mean-field behaviour are very hard to obtain and at present they only exist for the Casimir amplitudes in the form of the ε-expansion, where $\varepsilon = 4 - d$. The numerical quality of the ε-expansion when extrapolated to $\varepsilon = 1$ is very poor, so exact

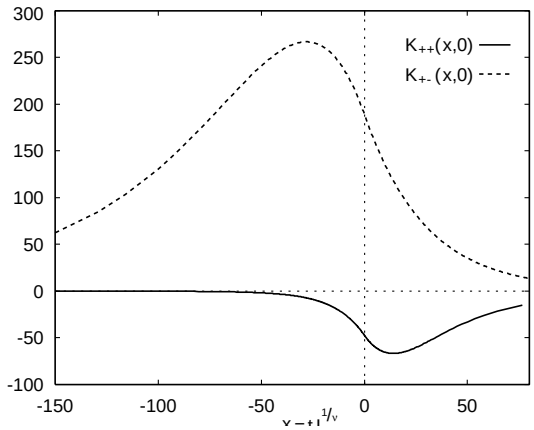

Figure 1. Scaling functions $K_{++}(x, 0)$ (solid line) and $K_{+-}(x, 0)$ (dashed line) taken from figure 1 of reference [26]. The x-range influenced by the bulk critical point $x = 0$ is very broad and the asymptotic decay for $x \to \pm\infty$ is dominated by an exponential. Note that $K_{++}(x, 0)$ and $K_{+-}(x, 0)$ take their extreme values at $x \simeq 10$ and $x \simeq -25$, respectively.

results for $d = 2$ have been included in order to obtain an interpolation formula for the Casimir amplitudes for $d = 3$. The values for Δ_{++}, Δ_{+-}, and Δ_{O+} obtained in this way agree reasonably well with Monte Carlo estimates (see section 3) [26]. The ε-expansion for Δ_{++} and Δ_{+-} has recently received some independent confirmation from local functional methods [28] which also provide reliable numerical estimates for $d = 3$ (see table 1 in section 3).

Apart from usual critical points, for which the upper critical dimension is $d_u = 4$, tricritical points in liquid mixtures with more than two components [29] and in ^{3}He–^{4}He mixtures (see section 6 of reference [3]) also provide an opportunity for experimental tests of the Casimir force. A theoretically appealing feature of a tricritical point is that its upper critical dimension is $d_u = 3$, so exact results for $d = 3$ can be obtained essentially from a mean-field or a Gaussian theory. If, for example, Dirichlet boundary conditions are the correct ones for a ^{3}He–^{4}He mixture in a film at the tricritical point, then the Casimir amplitude $\Delta_{OO} = -\zeta(3)/(8\pi) \simeq -0.0478$ given in equation (1.6) is also the right one for this system. There is, however, some debate concerning the correct boundary conditions for tricritical ^{3}He–^{4}He mixtures [29]. The result obtained for Δ_{++} at a tricritical point for $d = 3$ contains a logarithmic factor which is absent below the upper critical dimension d_u and which introduces a dependence on a microscopic length scale into the Casimir amplitude [29]. This dependence is very weak and Δ_{++} at tricriticality is expected to be about seven times larger than the corresponding amplitude at a usual critical point [29].

2.2.2. Curved geometries. In view of experimental set-ups for, e.g., atomic force microscopy it is desirable to consider geometries other than films, because two plates cannot be kept parallel accurately enough during force measurements. Curved geometries like a sphere in front of a planar wall or two spheres are much more convenient to control experimentally and are also much closer to reality in, e.g., colloidal suspensions [30] (see also reference [31]). Some theoretical effort has therefore been made on the investigation of these curved geometries, where conformal invariance considerations have proved to be a very powerful tool at the critical point [32]. If $\mathcal{F}_{ab}(r, R_1, R_2)$ denotes the free energy of a critical fluid in which two spheres with radii R_1 and R_2 at a centre-to-centre distance $r > R_1 + R_2$ are immersed, then

the Casimir interaction $\delta\mathcal{F}_{\rm ab}$ takes the scaling form [32]

$$\delta\mathcal{F}_{\rm ab}(r, R_1, R_2) \equiv \mathcal{F}_{\rm ab}(r, R_1, R_2) - \mathcal{F}_{\rm ab}(r = \infty, R_1, R_2) = k_B T_{c,b} F_{\rm ab}(\kappa) \tag{2.7}$$

where ab denotes the combination of surface universality classes and κ is the conformally invariant cross ratio

$$\kappa = (2R_1R_2)^{-1}|r^2 - R_1^2 - R_2^2|. \tag{2.8}$$

Note that the cases of two separate spheres in an unbounded critical medium and a single sphere inside a critical medium of spherical shape are conformally equivalent and are therefore governed by the same universal scaling function $F_{\rm ab}(\kappa)$ [32]. For large R_1 and R_2 at fixed surface-to-surface distance $D = r - R_1 - R_2$, one obtains from the limit of parallel plates [32]

$$\delta\mathcal{F}_{\rm ab}(r, R_1, R_2) = k_B T_{c,b} S_d \Delta_{\rm ab} [2(D/R_1 + D/R_2)]^{-(d-1)/2} \tag{2.9}$$

where S_d is the surface area of the unit sphere in d dimensions and $\Delta_{\rm ab}$ is the Casimir amplitude for parallel plates. In the opposite limit $r \gg R_1, R_2$ the presence of the spheres can be taken into account by the small-sphere expansion [32] which yields

$$\delta\mathcal{F}_{\rm ab}(r, R_1, R_2) = -k_B T_{c,b} \frac{A_{\rm a}^{\psi} A_{\rm b}^{\psi}}{B_{\psi}} \left(\frac{R_1 R_2}{r^2}\right)^{x_{\psi}} \tag{2.10}$$

where $\psi = \phi$ is the order parameter if both a = b = E indicate the extraordinary surface universality class. In this case the scaling exponent x_{ψ} is the scaling exponent of the order parameter $x_{\phi} = \beta/\nu$ ($\simeq$0.517 for the Ising model for $d = 3$). If only one of the surfaces is not characterized by the extraordinary surface universality class, the operator ψ is given by the local energy density ϕ^2 and x_{ψ} is the corresponding scaling exponent $x_{\phi^2} = d - 1/\nu$ ($\simeq$1.41 for the Ising model for $d = 3$). The amplitudes $A_{\rm a}^{\psi}$ and $A_{\rm b}^{\psi}$ are the amplitudes of the critical profiles $\langle\psi(z)\rangle^{s}_{\infty/2} = A_s^{\psi}(2z)^{-x_{\psi}}$, s = a, b, of the operator ψ in a semi-infinite system bounded by a planar surface of type s. The amplitude B_{ψ} is the amplitude of the $\psi\psi$-correlation function in unbounded space. Although none of these amplitudes is universal individually, their combination in equation (2.10) is universal and its value for various surface types is exactly known for the Ising universality class for $d = 2$. In $d = 4 - \varepsilon$ dimensions estimates can be calculated from a renormalization group analysis of the Ginzburg–Landau model [32]. Note that equations (2.7), (2.9), and (2.10) only hold at the critical point. The Casimir interaction according to equation (2.10) is in fact very long ranged. For the extraordinary surface universality class it decays about as slowly as the Coulomb interaction. In all other cases the decay is faster, but it is still slower than the decay of, e.g., dipolar interactions.

The full functional form of the scaling functions $F_{++}(\kappa)$, $F_{+-}(\kappa)$, $F_{+\rm SB}(\kappa)$, and $F_{+\rm O}(\kappa)$ has been calculated within mean-field theory from the stress tensor in the concentric sphere geometry [33]. As for the case of parallel plates, F_{++} and $F_{+\rm SB}$ are negative (attractive Casimir force), whereas F_{+-} and $F_{+\rm O}$ are positive (repulsive Casimir force). The boundary conditions ab = OO, O SB, and SB SB have been treated within the Gaussian model, where $F_{\rm OO}(\kappa) = F_{\rm SB\ SB}(\kappa) < 0$ and $F_{\rm O\ SB}(\kappa) > 0$ has been found. Although the analytic information from mean-field or Gaussian theory is quite limited, the combination of these results with exact results for $d = 2$ yields fairly reliable estimates for ab = ++, +−, +O, and OO within the Ising universality class for $d = 3$ [33]. Higher-order calculations beyond the mean-field or the Gaussian approximation, respectively, for the concentric geometry are extremely demanding and results are not available. Finally, we note that the sphere–planar-wall (SPW) geometry can also be obtained from the concentric geometry by a conformal mapping [33].

So far, conformal invariance could be used to obtain the scaling functions of the Casimir interaction for various geometries with spherical surfaces. If the correlation length ξ is

finite, conformal invariance no longer holds. Moreover, if all length scales ξ, r, R_1, and R_2 are comparable, small-sphere expansions cannot be made any longer and a new calculation is required for every geometry. In this case even mean-field results can only be obtained numerically [34]. So far, this has only been done in detail for the SPW geometry ($R_1 = R$, $R_2 \to \infty$, $D = r - R_1 - R_2 =$ constant) with ++ boundary conditions and at arbitrary temperature near the critical point for Ising-like systems [34]. We restrict the discussion to the case $T > T_{c,b}$, where the correlation length $\xi_+ = \xi_+^0 t^{-\nu}$ governs the decay of the order parameter correlation function in real space. The Casimir force can be cast into the scaling form [34]

$$\mathcal{K}_{++}(t, D, R) = \frac{k_B T_{c,b}}{R} K_{++}^{+}(x_+ = D/\xi_+, y_+ = R/\xi_+) \tag{2.11}$$

where a corresponding scaling function $K_{++}^{-}(x_-, y_-)$ governs the scaling behaviour of the Casimir force below $T_{c,b}$. The scaling functions are obtained from the mean-field evaluation of the stress tensor which requires the knowledge of the order parameter profile within mean-field theory. The order parameter profile is obtained from a numerical solution of the Euler–Lagrange equation for equation (2.1) in the presence of parallel and infinite surface fields which dictate the boundary conditions. The functional form of $K_{++}^{+}(x_+, y_+)$ is illustrated in figure 2. As for the case of parallel plates, the Casimir force is attractive and takes its maximum value above $T_{c,b}$. The true position of the maximum is somewhat concealed in figure 2 due to the normalization factor $\Delta^{5/2}$, which is required in order to absorb the divergence of K_{++}^{+} for $\Delta = D/R \to 0$. In this limit the Derjaguin approximation becomes valid, where the Casimir force is represented as an integral over parallel-plate contributions. Each of these 'parallel plates' in the d-dimensional SPW geometry is an infinitesimal annulus of width $\mathrm{d}\rho$ and radius ρ which is located on the surface of a paraboloid in order to approximate the sphere near the wall. The distance of one of these annuli from the wall is then given by $L(\rho) = D + \rho^2/(2R)$, where the integration is performed from $\rho = 0$ to $\rho = \infty$ [34]. Note that this approximation is only valid for forces which decay sufficiently fast as $L(\rho) \to \infty$. The amplitude of the Derjaguin approximation to the Casimir force at $T = T_{c,b}$ is indicated by the open circle in figure 2, where all solid lines meet. The dashed line corresponds to the small-sphere expansion

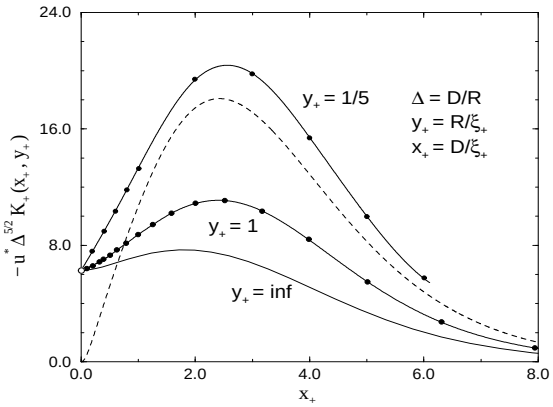

Figure 2. Scaling function $K_{++}^{+}(x_+, y_+)$ as a function of x_+ for various values of y_+ (solid lines). The prefactor $\Delta^{5/2}$ absorbs the divergence of the scaling function in the limit $\Delta \to 0$, where the Derjaguin approximation becomes valid (see the main text). The fixed-point value u^* of the renormalized coupling constant is required as an additional normalization due to the mean-field character of the calculation. The dashed line corresponds to the small-sphere expansion, which is shown here for $y_+ = 1/5$. The exponential decay of the scaling function sets in at $x_+ \simeq 4$.

to leading order, where $y_+ = 1/5$ has been used instead of the correct choice $y_+ = 0$, for which a factor Δ^2 is required for proper normalization [34].

The presence of small external fields can be used to drive, e.g., a critical binary liquid mixture slightly away from the critical concentration. Within the small-sphere expansion the Casimir energy between two spheres (colloidal particles) turns out to be nonsymmetric with respect to deviations from the critical concentration, such that the Casimir force is enhanced when the concentration of the component preferentially adsorbed by the colloids is reduced [34]. This asymmetry is consistent with the asymmetry found experimentally in the flocculation phase diagram of colloidal suspensions [30].

The concentric sphere geometry for ++ boundary conditions has also been considered at tricritical points [29], where the principle of conformal invariance can be used as well (see reference [33]). The expressions for the Casimir forces in the different geometries are similar to the ones obtained for critical points [33] apart from the logarithmic dependence on a microscopic length scale. The scaling function of the Casimir force depends on the conformally invariant cross ratio given by equation (2.8). In the range of distances D where force measurements with the atomic force microscope appear to be feasible, both Casimir and van der Waals forces are essentially governed by the parallel-plate limit of the curved geometries studied here [29]. Corresponding investigations of the Casimir forces away from the tricritical point have apparently not been performed.

Finally, we mention that a diluted polymer solution may also serve as a critical medium which mediates long-ranged forces between, e.g., colloidal particles [35]. Systematic investigations, however, are still at an early stage and the description of these is beyond the scope of this article.

3. Computer simulation

Computer simulations of forces in liquid films have been performed in the past primarily with regard to the microscopic mechanisms of friction, adhesion, and lubrication, where both Monte Carlo [36] and molecular dynamics methods [37] have been used (see reference [6] for background material and more details). With regard to the Casimir force in critical or correlated fluids the situation is less satisfactory. The computational effort involved in such calculations is substantial and consequently only very few Monte Carlo studies of the critical Casimir effect exist. Only rectangular geometries have been considered so far for $d = 3$, because the currently available system sizes do not provide sufficient resolution to investigate curved geometries.

3.1. Casimir amplitudes

The first systematic attempt to measure the Casimir amplitudes of Ising and Potts models in a film geometry is based on a splitting procedure for lattice models *at* criticality [38]. The systems contain $M^{d-1} \times L$ lattice sites, where an aspect ratio of $M/L = 6$ turns out to be sufficient to approximate the film geometry. In the lateral directions periodic boundary conditions are always applied. A seam is introduced into the system Hamiltonian, which continuously weakens existing bonds and simultaneously establishes new bonds until the lattice is cut into two halves of size $M^{d-1} \times L/2$. Histograms taken in the seam energy give access to the change of the free energy as a function of the seam strength [38], which finally yields the total change of the free energy when the lattice is cut in two. For periodic boundary conditions this method yields the Casimir amplitude Δ_{per} directly. For other boundary conditions the knowledge of Δ_{per} is required as input information [38]. The method works very well for $d = 2$ for critical

Potts models with $q = 2$, 3, and 4 and has subsequently been applied to the Ising model for $d = 3$ with periodic boundary conditions [38] and with surface fields [26]. A summary of the currently available estimates for the Casimir amplitudes from various sources is displayed in table 1 which includes older Migdal–Kadanoff estimates taken from reference [39]. Apart from the well known numerical uncertainties regarding the extrapolation of the ε-expansion and the Migdal–Kadanoff renormalization scheme, the agreement between the estimates for each of the amplitudes is encouraging. Especially for Δ_{++} and Δ_{+-}, where the ε-expansion and the Migdal–Kadanoff scheme are particularly unreliable, the other estimates are fairly consistent. There are still some prospects for improving the Migdal–Kadanoff estimates also for these cases, but final results are not yet available [40]. It would also be desirable to obtain estimates for the Casimir amplitudes from a field theoretic calculation in $d = 3$ dimensions directly, but attempts in this direction have not yet been made. The Monte Carlo estimates for Δ_{++} and Δ_{+-} are obtained by extrapolating the individual data to infinite lattice size [26]. For Δ_{+-} this works rather well, but for Δ_{++} substantial systematic uncertainties remain and additional data for larger systems are required to obtain a reliable extrapolation (see figures 4 and 5 in reference [26]). At present local functional methods as set up in reference [28] seem to provide the most reliable estimates for Δ_{++} and Δ_{+-}, because the dimensional dependence of these amplitudes appears to be captured rather well by the local free-energy functional. Finally, we note that the Casimir amplitudes may also be accessible by exploring the order parameter distribution at the critical point [41]. So far this method has only been used for fully finite cubic geometries; generalizations to other geometries have not yet been explored.

Table 1. Casimir amplitudes for the Ising universality class for $d = 3$. The values labelled $\varepsilon = 1$ are obtained by extrapolating the ε-expansion for $N = 1$ to $\varepsilon = 1$ [26]. The values labelled $d = 3$ are obtained from Padé-type approximants for $d = 3$ ($\varepsilon = 1$) [26]. The Monte Carlo estimates obtained from the algorithm presented in reference [38] are labelled by 'MC'. Statistical errors (one standard deviation) are indicated by the figures in parentheses. The last two lines show estimates taken from references [39] and [28].

	Δ_{per}	$\Delta_{\mathrm{O,O}}$	$\Delta_{+,+}$	$\Delta_{+,-}$	$\Delta_{\mathrm{SB},+}$	$\Delta_{\mathrm{O},+}$
$\varepsilon = 1$	−0.1116	−0.0139	−0.173	1.58	−0.093	0.165
$d = 3$	−0.1315	−0.0164	−0.326	2.39		0.208
MC	−0.1526(10)	−0.0114(20)	−0.345(16)	2.450(32)		0.1873(70)
Reference [39]		−0.015	0	0.279	0.017	0.051
Reference [28]			−0.428	3.1		

3.2. Off-lattice models and the wetting scenario

A great drawback of the Monte Carlo method introduced in reference [38] is that it cannot be generalized to temperatures $T \neq T_{c,b}$. The method is based on the measurement of free-energy differences, which correspond to linear combinations of the scaling functions at different scaling arguments for $T \neq T_{c,b}$. Data of extremely high accuracy would be required to disentangle the individual contributions to the measured free-energy difference. An alternative approach is to mimic the complete wetting scenario (see reference [42]) near the critical end-point of the demixing transition in a binary liquid mixture in a computer simulation [43]. The order parameter in this case is the concentration of the mixture ($N = 1$, Ising universality class) rather than the density difference between liquid and gas, which is usually taken as the order parameter near the liquid–vapour critical point. In fact, temperature and pressure are adjusted such that the mixture is in its vapour phase very close to liquid–vapour coexistence but *far away* from the liquid–vapour critical point. The interplay between the interparticle

potential and the interaction between the particles and an external wall (substrate) may lead to the formation of a macroscopic liquid wetting layer of thickness L on the substrate at some temperature T_w below the liquid–vapour critical point [42]. The problem in the preparation of such a complete wetting layer for a binary mixture is to find a system, i.e., parameter values for a simulation, such that the critical end-point of the demixing transitions is *inside* the complete wetting regime, where the macroscopic wetting layer remains stable (see reference [42] for more background information on wetting transitions). The Casimir effect associated with the critical demixing transition in a liquid layer of thickness L can then be studied. The suggestion of probing the Casimir effect in complete wetting layers near critical end-points was first made by Nightingale and Indekeu [44] and was later worked out in more detail, as the first estimates for the scaling functions of the Casimir force became available [45] (see also section 6 of reference [3]). The main objective of such a simulation, however, is to obtain more insight into the Casimir effect in a more realistic off-lattice model with Lennard-Jones interactions, which would be the typical situation in an experiment [43]. Simulations have been performed for a symmetric binary liquid characterized by the Lennard-Jones interparticle potential

$$u_{ij}(r) = 4\epsilon_{ij}\left[\left(\frac{\sigma_{ij}}{r}\right)^{12} - \left(\frac{\sigma_{ij}}{r}\right)^{6}\right] \tag{3.1}$$

for two particle species $i, j = 1, 2$, where the choices $\sigma_{ij} = \sigma$ for the hard-core parameters and $\epsilon_{11} = \epsilon_{22} = \epsilon$, $\epsilon_{12} = 0.7\epsilon$ for the well depth parameters have been made. Note that with these choices the system is invariant under the species exchange $1 \leftrightarrow 2$ and therefore the chemical potentials of both species have been set equal, $\mu_1 = \mu_2 = \mu$, from the outset. The simulations are performed on a box of size $P^2 \times D$, where periodic boundary conditions are applied in the x- and y-directions and two hard walls are specified in the z-direction, one at $z = 0$ and one at $z = D$. The wall at $z = 0$ is characterized by the attractive potential

$$V(z) = \epsilon_w\left[\frac{2}{15}\left(\frac{\sigma}{z}\right)^{9} - \left(\frac{\sigma}{z}\right)^{3}\right] \tag{3.2}$$

which acts *equally* on the particle species [43]. The interparticle interactions are truncated at $R_c = 2.5\sigma$, whereas no range cut-off is employed for $V(z)$. The phase diagram of the system is spanned by the parameters μ/k_BT, ϵ/k_BT, and ϵ_w/k_BT. The system sizes used are $P = 12.5\sigma$, 15σ, and 17.5σ, where $D = 40\sigma$ in all cases [43]. The parameters are chosen such that (i) a complete wetting layer forms on the substrate and (ii) the end-point of the critical demixing transitions is inside the complete wetting regime (see above). In order to obtain a sufficiently thick wetting layer ($L \geqslant 10\sigma$) the undersaturation of the vapour $\delta\mu/\mu$ must be tuned to about 10^{-3}. The data acquisition is strongly hampered by large fluctuations of the liquid–vapour interface position (capillary waves) which also lead to a substantial slowing down of the algorithm. Furthermore, the data are strongly affected by lateral finite-size effects, because the capillary-wave fluctuations also limit the lateral system sizes attainable with reasonable computational effort [43].

The equilibrium thickness L of the wetting layer (see also section 4) minimizes the effective interface potential $\omega(l)$ [42, 43] as a function of the test layer thickness l, which is a variational parameter in the spirit of mean-field theory. The effective interface potential is given by

$$\omega(l) = l(\rho_l - \rho_v)\,\delta\mu + \sigma_{wl} + \sigma_{lv} + \delta\omega(l) \tag{3.3}$$

where ρ_l and ρ_v denote the liquid and vapour densities, respectively. The interfacial tensions σ_{wl} between the wall ($z = 0$) and the liquid and σ_{lv} between the liquid and the vapour do not depend on l. The last term $\delta\omega(l)$ contains the contributions of all interactions across the

wetting layer and it depends on the boundary conditions. By construction there are no surface fields acting on the model liquid which break the $1 \leftrightarrow 2$ symmetry between the particle species, i.e., $\boldsymbol{H}_1 = 0$ (see equation (2.2) for $N = 1$). However, the wall potential given by equation (3.2) acts like a *negative* surface enhancement c (see equation (2.2)), which supports demixing near the surface, whereas the liquid–vapour interface acts as a free surface ($c > 0$) due to the internal $1 \leftrightarrow 2$ symmetry of the model liquid. The surface universality classes should thus be characterized by the combination (ab) = (O+). *At* $T = T_{cep}$, $\delta\omega(l)$ is therefore used in the form [43]

$$\delta\omega(l) = \frac{W}{l^2} + k_B T_{cep}\left(\frac{\Delta_{\mathrm{O}+}}{l^2} + \frac{2l\Delta_{per}}{P^3}\right) \tag{3.4}$$

where the Hamaker constant $W \simeq 2.5 k_B T_{cep}$ governs the van der Waals contribution to the interaction potential and the Casimir amplitude $\Delta_{\mathrm{O}+} \simeq 0.2$ (see table 1) governs the Casimir interaction for a symmetric liquid mixture [43]. Note that positive Casimir amplitudes (repulsion) lead to a critical *thickening* of the wetting layer, whereas negative Casimir amplitudes (attraction) lead to a critical *thinning* of the wetting layer. The last term in equation (3.4) is governed by the Casimir amplitude $\Delta_{per} \simeq -0.15$. It provides an order-of-magnitude account of the aforementioned lateral finite-size effects which can be treated as a shift of the undersaturation $\delta\mu$. In the limit $P \gg l$ (film geometry), the critical thickening of the wetting layer is given by [43]

$$L_c/L_0 = (1 + k_B T_{cep}\Delta_{\mathrm{O}+}/W)^{1/3} \tag{3.5}$$

where $L_c = L(T_{cep})$ and L_0 is the equilibrium layer thickness outside the critical regime. The measured film thickness $L(T)$ versus temperature is shown in figure 3. The critical thickening of the wetting layer $L_c/L_0 - 1$ for the largest system (lowest curve in figure 3) is of the order of 3% which is in rough agreement with equation (3.5). The apparent reduction of the critical thickening with increasing lateral system size can be explained semiquantitatively by the lateral finite-size correction included in equation (3.4). Further studies of off-lattice models like this are certainly desirable; however, algorithmic improvements for the treatment of capillary waves will be indispensable for future progress.

3.3. The lattice stress tensor

The computer simulation of the complete wetting scenario is quite successful, but by design it only gives an indirect account of the scaling functions K of the Casimir force. As already described in section 2, the most direct access to the Casimir force is given by the thermal average of the *stress tensor* and it would therefore be most convenient to have a lattice expression for the stress tensor available for spin models. Such expressions can indeed be obtained and successfully used in Monte Carlo simulations for lattice models for $d = 2$ [46]. The basic idea behind the construction of the stress tensor is the same as in continuum theory: one calculates the response of the free energy to a nonconformal mapping of the system, e.g., an *anisotropic* rescaling of the coupling constants. For example, one may choose $J_x = J_x(\lambda)$, $J_y = J_y(\lambda)$ with $J_x(0) = J_y(0) = J$ and $J_x(\lambda) = J_y(-\lambda)$ on a square lattice, such that the critical temperature does not depend on λ. For the Ising model for $d = 2$ this procedure yields, e.g., the xx-component of the lattice stress tensor at lattice site (i, j) in the form [46]

$$t_{xx}(i, j) = -J_x'(0)(S_{i,j}S_{i+1,j} - S_{i,j}S_{i,j+1}) \tag{3.6}$$

where $J_x'(0)$ is the derivative of $J_x(\lambda)$ at the isotropic point $\lambda = 0$. The thermal averages $\langle t_{xx}\rangle$ of equation (3.6) and $\langle T_{xx}\rangle$ of the stress tensor in conformal field theory are related by $\langle t_{xx}\rangle = \alpha\langle T_{xx}\rangle$ up to corrections to scaling, where α is exactly known for the 2D Ising

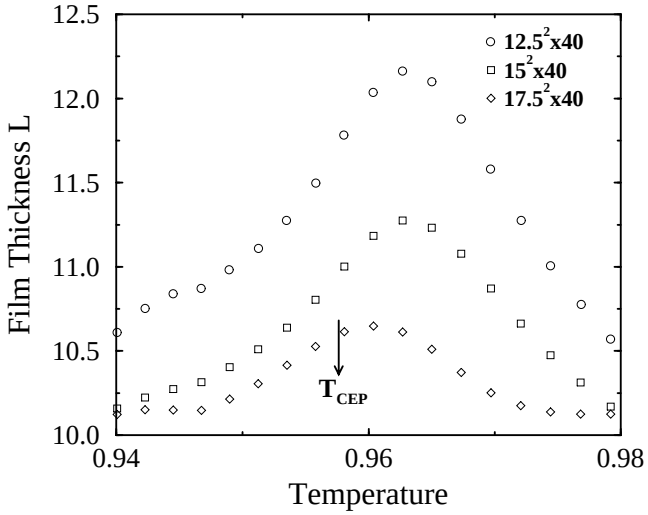

Figure 3. Thickness of the wetting layer as a function of temperature in reduced Lennard-Jones units along a path parallel to the liquid–vapour coexistence line. Data are shown for each of the three system sizes studied. The results were obtained from multihistogram extrapolation of simulation data accumulated at three points on this path, corresponding to temperatures $T = 0.946$, 0.958, 0.97 (see reference [43]).

model. For periodic boundary conditions in a strip geometry, equation (3.6) can be used to measure the Casimir amplitude Δ_{per} (i.e., the conformal anomaly number c) and two or more scaling dimensions for the Ising model and other models if equation (3.6) is generalized accordingly [46]. For lattice models for $d = 2$, conformal field theory provides sufficient background information that the desired quantities can be extracted from elaborate fitting procedures [46]. Although equation (3.6) can be readily generalized to $d = 3$, additional information from conformal field theory, which is vital for the data interpretation for $d = 2$, is no longer available. Furthermore, $\langle t_{xx} \rangle$ still contains surface contributions for nonperiodic boundary conditions, because the surface tensions will depend on the anisotropy parameter λ even if the critical point does not. However, for periodic boundary conditions $\langle t_{xx} \rangle$ is at least proportional to the Casimir force and some preliminary studies for the XY model in an $M^2 \times L$ geometry in $d = 3$ dimensions look promising [47], although high statistics is already needed for small systems.

4. Experiments

Experimental verifications of the Casimir effect in critical liquids are exceedingly difficult, because data of high accuracy are required and both samples and apparatus must be prepared with great care. At present, two lines of approach are considered, namely the wetting scenario sketched already in section 3 and direct force measurements by atomic force microscopes (AFM).

4.1. Wetting experiments

For a wetting experiment in the vicinity of a critical point a fluid is required which possesses a critical end-point on the liquid–vapour coexistence line. One option for this set-up is provided by ^{4}He near its lower λ-point [48]. For this system the interaction part of the effective interface potential (see equations (3.3) and (3.4)) must be modified according to the universality class of the λ-transition in ^{4}He (XY, $N = 2$). The boundary conditions at the two interfaces of the wetting layer seem to be very well approximated by Dirichlet boundary conditions (O surface universality class). This leads to [45, 48]

$$\delta\omega(l) = \frac{W}{l^2}\left(1 + \frac{l}{L_x}\right)^{-1} + \frac{k_B T_\lambda}{l^2}\theta_{\mathrm{OO}}(tl^{1/\nu}, \delta\mu\, l^{\beta\delta/\nu}) \tag{4.1}$$

where $L_x \simeq 193$ Å denotes the crossover length to retardation [49], and θ_{OO} is the scaling function of the Casimir potential for the ordinary surface universality class (see equation (2.3)). Note that W and L_x depend on the dielectric properties of the adsorbate and the substrate. From equations (3.3) and (4.1) one expects a critical *thinning* of the wetting layer thickness, because $\theta_{\mathrm{OO}} < 0$. Note that the second scaling argument of θ_{OO} captures off-coexistence effects due to the undersaturation $\delta\mu$ of the ^{4}He vapour. At the λ-point ($t = 0, \delta\mu = 0$) one has $\theta_{\mathrm{OO}}(0, 0) = \Delta_{\mathrm{OO}} \simeq -0.024$ which results in a critical thinning of $\sim$0.3% for standard substrates like, e.g., copper [3, 45]. In the experimental set-up a stack of five copper capacitors is placed inside a cell which contains liquid ^{4}He at the bottom. The surfaces of the capacitor provide the substrate potential (see equation (3.2)) and their elevation h in the gravitational field controls the undersaturation $\delta\mu \sim \rho_v g h$ of the ^{4}He vapour. The layer thickness is obtained from high-precision measurements of the capacitance of each of the capacitors as a function of temperature. The wetting behaviour of ^{4}He is extremely sensitive to the surface morphology of the copper plates. In particular, microscopic scratches and dust particles lead to localized condensation of ^{4}He on the surface which results in an overestimation of the thickness. Moreover, surface roughness leads to an enhanced surface area which also increases the amount of liquid ^{4}He on the substrate. Even with the most advanced polishing techniques these effects cannot be avoided completely and therefore also the experimental verification of the DLP theory of dispersion forces [5] remains a challenge. Nevertheless, the experimental data for the film thinning show a pronounced minimum well below T_λ which is given by the specific value $x_m = -9.2 \pm 0.2$ of the first scaling argument $x = tL^{1/\nu}$ in equation (4.1). This value coincides with the minimum of the scaling function $K_{\mathrm{OO}}(x, y)$ of the Casimir force with respect to x. The experimental estimate of $\vartheta(x) \equiv K_{\mathrm{OO}}(x, y = 0)$ extracted from the data is displayed in figure 4, which does not show the expected data collapse for the scaling function K_{OO}. On the contrary, a systematic trend in the data as a function of the elevations h of the capacitors is visible as shown in the inset of figure 4. One possible explanation may be given by off-coexistence effects, which would require the second scaling variable $y = \delta\mu\, L^{\beta\delta/\nu}$ in equation (4.1) for data collapse. If a linear dependence of K_{OO} on y is assumed, the deviations from data collapse are indeed drastically reduced [48]. Another option is provided by the introduction of a roughness correction factor as suggested in reference [18], which leads to a similar improvement [48]. However, it is evident from figure 4 that there are no appreciable deviations from data collapse for $x \geqslant 0$, where a quantitative prediction for $K_{\mathrm{OO}}(x, y = 0)$ exists [3, 45]. The comparison is displayed in figure 5 which shows reasonable agreement between the data and the prediction. Finally, we note that a finite thinning effect remains visible for temperatures further below T_λ, as one would expect from the presence of Goldstone modes [18, 23]. The overall shape of K_{OO} is manifestly nonmonotonic in contrast to the recently stated monotonicity hypothesis for O($N > 1$)-symmetric spin models [23].

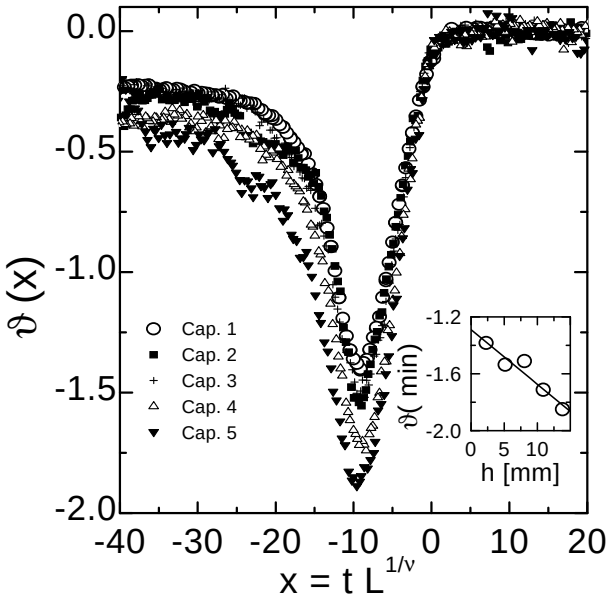

Figure 4. Scaling function $\vartheta(x) \equiv K_{OO}(x, 0)$ as a function of x. The magnitude of the minimum increases systematically with the height h of the capacitor. The measured layer thickness L is roughly between 300 Å and 600 Å depending on the capacitor index 1–5. The inset shows the value of $\vartheta(x)$ at the minimum versus height. The uncertainty in the vertical scale is 2–10% (taken from reference [48]).

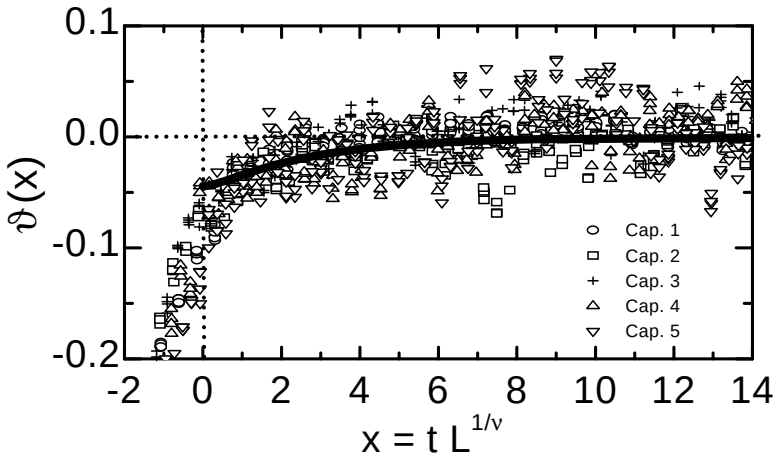

Figure 5. A blow-up of the region $x \geqslant 0$ in figure 4. Every other data point is shown. The solid line shows the prediction from figure 9 in reference [45] (taken from reference [48]).

A second option for a wetting experiment in the vicinity of a critical end-point is provided by binary liquid mixtures near the critical end-point T_{cep} (see section 3) of the line of second-order demixing transitions [50] (see references [42, 45] for complete phase diagrams). The physical situation is very much like that for ^{4}He near the lower λ-point, except that both the bulk and surface universality classes are different here. The second-order demixing transition

is characterized by a scalar order parameter (concentration), so the system is in the Ising ($N = 1$) universality class. The substrate material as well as the liquid–vapour interface, which provide the boundaries of the system, usually show some preferential affinity for one of the two components of the mixture; i.e., the concentration (order parameter) departs from its critical bulk value in the vicinity of the surfaces. This phenomenon is known as critical adsorption (see, e.g., reference [12]) and it is captured by the *extraordinary* surface universality class. In the experiment [50] a molecularly smooth (100) Si wafer (n-type, phosphorus doping) covered with a SiO_2 layer of $\sim$2.0 nm thickness is used, which is suspended vertically inside a Pyrex cell. The elevation h of the substrate above the bulk liquid at which the wetting layer thickness is measured controls the undersaturation of the vapour. The reduction of temperature gradients for wetting agents other than superfluid ^{4}He is a quite demanding task and it substantially complicates the preparation of the cell and the sample [50]. In this experiment two organic mixtures have been used, namely methanol + hexane (MH) and 2-methoxy-ethanol + methylcyclohexane (MM). In MH the methanol component is adsorbed at the Si wafer, whereas hexane is adsorbed at the liquid–vapour interface of the wetting layer. In MM the situation is similar: the 2-methoxy-ethanol is adsorbed at the Si wafer, whereas the methylcyclohexane is adsorbed at the liquid–vapour interface. The wetting layers of both mixtures are therefore characterized by the scaling functions θ_{+-} of the Casimir potential. The interaction contribution $\delta\omega(l)$ to the effective interface potential $\omega(l)$ in this case is assumed to be of the form [50]

$$\delta\omega(l) = \frac{W}{l^2} - A\mathrm{e}^{-l/d} + \frac{k_B T_{cep}}{l^2}\theta_{+-}(tl^{1/\nu}, 0) \tag{4.2}$$

where retardation and off-coexistence effects are neglected. The exponential contribution to equation (4.2) is due to the presence of the hard wall, which structures the adsorbed fluid over a molecular distance d. The critical temperature T_{cep} is about 300 K [50]. At the moment only mean-field results [26] and exact results for $d = 2$ [27] exist for the scaling function K_{+-} of the Casimir force. In order to obtain reasonable estimates also in $d = 3$ dimensions, at least the one-loop corrections are required, which only exist for $\Delta_{+-} = 2K_{+-}(0, 0)$ at the moment (see reference [26] and table 1). From equation (3.5) and typical values for T_{cep} and the Hamaker constant W, one expects a critical thickening $L_c/L_0 \geqslant 2$ of the wetting layer, when the estimate $\Delta_{+-} \simeq 2.4$ (see table 1) is used. As T_{cep} is approached from above, a critical thickening of the wetting layer consistent with this expectation has been found in the experiment and the data for $K_{+-}(x, 0)$ are indeed consistent with scaling [50]. As a function of the scaling variable $y \equiv L/\xi_+$ the scaling function $\vartheta_{+-}(y) \equiv K_{+-}(x = (\xi_0^+ y)^{1/\nu}, 0)$ is shown in figure 6. A comparison between $\vartheta_{+-}(y)$ *at* and away from the critical composition is shown in the inset for MH. The shape of $\vartheta_{+-}(y)$ shown in figure 6 resembles that of the mean-field estimate $K_{+-}(x, 0)$ for $x > 0$ shown in figure 1. However, the Hamaker constant W and therefore also the Casimir amplitude Δ_{+-}, which have been extracted from the data, are much smaller than anticipated. The reason for this discrepancy has not yet been fully understood. One possible explanation could be that the parameters of the system are not in the complete wetting regime, i.e., only *partial* rather than complete wetting [42] is achieved. Further studies are currently under way.

4.2. AFM measurements

As already mentioned in section 3, the theoretical investigation of critical fluids in curved geometries is, *inter alia*, motivated by the prospects of measuring the Casimir force directly with an AFM. At the moment only exploratory results are available [51] which have been obtained for the SPW geometry in liquid crystals (see references [19, 20]). In this study a

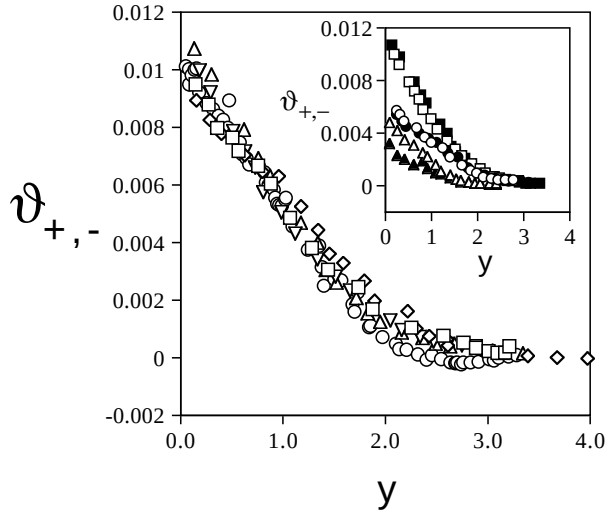

Figure 6. Universal scaling function $\vartheta_{+,-}(y)$, $y = L/\xi_+$, for the critical Casimir force. The symbols represent data at fixed elevations $h = 1.5$ mm (diamonds), $h = 3.3$ mm (squares) for MM and $h = 3.4$ mm (triangles), $h = 6.3$ mm (inverted triangles) for MH. In the inset the experimental function $\vartheta_{+,-}(y)$ for the system MH with the critical composition (squares), 5% excess hexane (circles), and 10% excess hexane (triangles) at two different heights (3.5 mm (open symbols) and 6.0 mm (solid symbols)) on a silicon wafer is shown.

temperature-controlled AFM has been used to measure the force between a sphere mounted on the cantilever tip of the AFM and a planar wall immersed in an 8CB liquid crystal near the isotropic–nematic phase transition. Above the transition in the isotropic phase an attractive force of the order of 10^{-10} N at a distance $D = 1$ nm $\pm$ 0.1 nm between the surface of the sphere ($R = 5$ μm) and the wall is detected only when the two surfaces are *moving apart*. This phenomenon is similar to the capillary force in AFM microscopy and it is interpreted as the adsorption of a nematically ordered layer of the liquid crystal on the surface of the sensing probe [51]. Slightly above the transition to the nematically ordered phase an additional attractive force of the order of 10^{-11} N is detected when the surfaces are *approaching* one another. This additional force is conjectured to be the Casimir force mediated by the onset of Goldstone modes of the nematic director field in the ordered phase [19, 51], where the boundary conditions are supplied by the type of anchoring of the nematic director on the surfaces [19]. Further quantitative studies of Casimir forces in critical and correlated liquids with this apparatus are certainly desirable. Finally, we note that the radiation pressure on a dielectric sphere in the evanescent field of totally reflected light has recently been measured using such AFM techniques [52].

5. Prospects for further investigations

The theoretical knowledge about Casimir forces in critical and correlated fluids which has been accumulated during the last ten years has become so detailed that the stage is set for experimental tests of various kinds. Wetting experiments near critical end-points have already proved to be a powerful tool for accomplishing this goal for quite a variety of fluids. Further studies in this direction are certainly highly desirable and the prospects for them are very good despite the substantial experimental challenges that one has to face. From the existing

theoretical work on curved geometries it has also become clear that the Casimir forces in critical and correlated fluids are within reach of current AFM designs. Preparation of the samples and temperature stabilization of the sample and the instrument again pose major challenges for AFM force measurements; however, the prospects of probing the Casimir effect quantitatively are also very good.

Conversely, the experimental approaches to the Casimir effect also pose new theoretical challenges. The problem of substrate roughness in wetting experiments has already been mentioned above and for the case of quenched roughness theoretical results already exist [18]. However, one of the boundaries of a wetting layer is a free liquid–vapour interface, which may undergo large-scale fluctuations due to capillary waves. What kind of corrections capillary waves as additional degrees of freedom impose on the critical Casimir potential is an open question. Quantitative estimates of these corrections are not only important for experiments, they would also aid the data interpretation of computer simulations for critical wetting layers. To what extent off-coexistence effects influence experimental and numerical wetting layer data is also a largely open problem. In this respect the recently explored numerical access to the stress tensor of lattice models may prove particularly useful [46, 47]. Finally, it should be mentioned that improvements of existing theoretical or numerical estimates for the scaling function K_{ab} of the Casimir force, in particular for the extraordinary surface universality class, in various geometries are still needed in order to extract the Casimir effect from experimental data as reliably as possible.

Although the history of the Casimir effect goes back more than half a century it has remained an active field of research. This article can therefore only provide a snapshot of current knowledge in this area rather than a complete picture. If this presentation could finally help to trigger or direct new research work in this field, then its main purpose would be fulfilled.

Acknowledgments

The author gratefully acknowledges stimulating discussions with M H W Chan, S Dietrich, R Garcia, M Kardar, B M Law, A Mukhopadhyay, and F Schlesener. Financial support for this work has been provided through the Heisenberg programme of the Deutsche Forschungsgemeinschaft, which is also gratefully acknowledged. The author expresses his special thanks to M H W Chan and R Garcia for providing copies of figures 4 and 5 and to B M Law and A Mukhopadhyay for providing a copy of figure 6 prior to publication.

References

[1] Casimir H B G 1948 *Proc. K. Ned. Akad. Wet.* **51** 793
Casimir H B G and Polder D 1948 *Phys. Rev.* **73** 360
Casimir H B G 1953 *Physica* **19** 846
Sukenik C I, Boshier M G, Cho D, Sandoghdar V and Hinds E A 1993 *Phys. Rev. Lett.* **70** 560
Lamoreaux S K 1997 *Phys. Rev. Lett.* **78** 5
[2] Plunien G, Müller B and Greiner W 1986 *Phys. Rep.* **134** 87
Mostepanenko V M and Trunow N N 1988 *Sov. Phys.–Usp.* **31** 965
Mostepanenko V M and Trunow N N 1997 *The Casimir Effect and its Applications* (Oxford: Clarendon)
Elizalde E and Romeo A 1991 *Am. J. Phys.* **59** 711
Milonni P W and Shih M-L 1992 *Contemp. Phys.* **33** 313
Spruch L 1996 *Science* **272** 1452
[3] Krech M 1994 *The Casimir Effect in Critical Systems* (Singapore: World Scientific)
[4] Kakazu K and Miyagi S 1998 *Prog. Theor. Phys.* **100** 687
[5] Lifshitz E M 1956 *Sov. Phys.–JETP* **2** 73
Dzyaloshinskii L E, Lifshitz E M and Pitaevskii L P 1961 *Adv. Phys.* **10** 165

Sabisky E S and Anderson C H 1973 *Phys. Rev.* A **7** 790
Schwinger J, DeRaad L L and Milton K A 1978 *Ann. Phys., NY* **115** 1
[6] Israelachvili J N 1992 *Intermolecular and Surface Forces* (New York: Academic)
[7] Elizalde E and Romeo A 1990 *Int. J. Mod. Phys.* A **5** 1653
Elizalde E 1990 *J. Math. Phys.* **31** 170
Kirsten K 1991 *J. Phys. A: Math. Gen.* **24** 3281
Dolan B P and Nash C 1992 *Commun. Math. Phys.* **148** 139
Leseduarte S and Romeo A 1996 *Europhys. Lett.* **34** 79
Leseduarte S and Romeo A 1996 *Ann. Phys., NY* **250** 448
[8] Svaiter N F and Svaiter B F 1990 *J. Math. Phys.* **32** 175
Svaiter N F and Svaiter B F 1992 *J. Phys. A: Math. Gen.* **25** 979
[9] Elizalde E 1994 *J. Phys. A: Math. Gen.* **27** L299
[10] Fisher M E and de Gennes P-G 1978 *C. R. Acad. Sci., Paris* B **287** 207
[11] Eisenriegler E, Krech M and Dietrich S 1996 *Phys. Rev.* E **53** 14 377
[12] Binder K 1983 *Phase Transitions and Critical Phenomena* vol 8, ed C Domb and J L Lebowitz (London: Academic) p 2
Diehl H W 1986 *Phase Transitions and Critical Phenomena* vol 10, ed C Domb and J L Lebowitz (London: Academic) p 76
Diehl H W 1997 *Int. J. Mod. Phys.* B **11** 3503
Diehl H W and Shpot M 1998 *Nucl. Phys.* B **528** 595
[13] Burkhardt T W and Diehl H W 1994 *Phys. Rev.* B **50** 3894
[14] Symanzik K 1981 *Nucl. Phys.* B **190** 1
[15] O'Connor D and Stephens C R 1994 *Phys. Rev. Lett.* **72** 506
Freire F, O'Connor D and Stephens C R 1994 *J. Stat. Phys.* **74** 219
Esser A, Dohm V and Chen X S 1995 *Physica* A **222** 355
Esser A, Dohm V, Hermes M and Wang J S 1995 *Z. Phys.* B **97** 205
Chen X S, Dohm V and Esser A 1995 *J. Physique* I **5** 205
Freire F, O'Connor D and Stephens C R 1996 *Phys. Rev.* E **53** 189
Chen X S, Dohm V and Talapov A L 1996 *Physica* A **232** 375
Chen X S, Dohm V and Schultka N 1996 *Phys. Rev. Lett.* **77** 3641
[16] Chen X S and Dohm V 1998 *Physica* A **251** 439
Chen X S and Dohm V 1998 *Eur. Phys. J.* B **5** 529
[17] Barber M N 1983 *Phase Transitions and Critical Phenomena* vol 8, ed C Domb and J L Lebowitz (London: Academic) p 145
Privman V 1994 *Finite Size Scaling and Numerical Simulation of Statistical Systems* ed V Privman (Singapore: World Scientific)
Privman V, Hohenberg P C and Aharony A 1991 *Phase Transitions and Critical Phenomena* vol 14, ed C Domb and J L Lebowitz (New York: Academic) p 1
[18] Li H and Kardar M 1991 *Phys. Rev. Lett.* **67** 3275
Li H and Kardar M 1992 *Phys. Rev.* A **46** 6490
Kardar M 1999 *APS Centennial Mtg (Atlanta, GA, March 1999)* talk
[19] Adjari A, Peliti L and Prost J 1991 *Phys. Rev. Lett.* **66** 1481
Adjari A, Duplantier B, Hone D, Peliti L and Prost J 1992 *J. Physique* **2** 487
Lyra M L, Kardar M and Svaiter N F 1993 *Phys. Rev* E **47** 3456
[20] Ziherl P, Zumer S and Podgornik R 1998 *Braz. J. Phys.* **28** 267
Ziherl P, Podgornik R and Zumer S 1998 *Chem. Phys. Lett.* **295** 99
[21] Allen S and Pathria R K 1989 *Can. J. Phys.* **67** 952
Allen S and Pathria R K 1991 *Can. J. Phys.* **69** 753
Brankov J G and Tonchev N S 1990 *J. Stat. Phys.* **60** 519
Brankov J G and Danchev D M 1991 *J. Math. Phys.* **32** 2543
Brankov J G and Danchev D M 1993 *J. Stat. Phys.* **71** 775
Danchev D M 1993 *J. Stat. Phys.* **73** 267
[22] Danchev D M 1996 *Phys. Rev.* E **53** 2104
[23] Danchev D M 1998 *Phys. Rev.* E **58** 1455
[24] Cardy J L 1987 *Phase Transitions and Critical Phenomena* vol 11, ed C Domb and J L Lebowitz (London: Academic) p 55
Itzykson C and Drouffe J-M 1992 *Statistical Field Theory* vol 2 (Cambridge: Cambridge University Press)
[25] McAvity D M and Osborn H 1993 *Nucl. Phys.* B **406** 655

[26] Krech M 1997 *Phys. Rev.* E **56** 1642
[27] Evans R and Stecki J 1994 *Phys. Rev.* B **49** 8842
[28] Borjan Z and Upton P J 1998 *Phys. Rev. Lett.* **81** 4911
[29] Ritschel U and Gerwinski M 1997 *Physica* A **243** 362
[30] Beysens D and Estéve D 1985 *Phys. Rev. Lett.* **54** 2123
[31] Carnie S L, Chan D Y C and Stankovich J 1994 *J. Colloid Interface Sci.* **165** 116
Johansson P and Apell P 1997 *Phys. Rev.* B **56** 4159
[32] Burkhardt T W and Eisenriegler E 1995 *Phys. Rev. Lett.* **74** 3189 and references therein
[33] Eisenriegler E and Ritschel U 1995 *Phys. Rev.* B **51** 13 717
[34] Hanke A, Schlesener F, Eisenriegler E and Dietrich S 1998 *Phys. Rev. Lett.* **81** 1885
Schlesener F 1997 *Diplomarbeit* Universität Wuppertal
[35] Eisenriegler E, Hanke A and Dietrich S 1996 *Phys. Rev.* E **54** 1134
[36] Schoen M, Diester D J and Cushman J H 1994 *J. Chem. Phys.* **100** 7707
[37] Das S K, Sharma M M and Schechter R S 1996 *J. Phys. Chem.* **100** 7122
[38] Krech M and Landau D P 1996 *Phys. Rev.* E **53** 4414
Mon K K 1985 *Phys. Rev. Lett.* **54** 2671
Mon K K 1987 *Phys. Rev.* B **35** 3560
[39] Indekeu J O, Nightingale M P and Wang W V 1986 *Phys. Rev.* B **34** 330
[40] Danchev D 1998 private communication
[41] Bruce A D 1995 *J. Phys. A: Math. Gen.* **28** 3345
[42] Dietrich S 1988 *Phase Transitions and Critical Phenomena* vol 12, ed C Domb and J L Lebowitz (London: Academic) p 1
[43] Wilding N B and Krech M 1998 *Phys. Rev.* E **57** 5795
[44] Nightingale M P and Indekeu J O 1985 *Phys. Rev. Lett.* **54** 1824
Nightingale M P and Indekeu J O 1985 *Phys. Rev. Lett.* **55** 1700
Lipowski R and Seifert U 1985 *Phys. Rev.* B **31** 4701
Lipowski R and Seifert U 1985 *Phys. Rev. Lett.* **55** 1699
[45] Krech M and Dietrich S 1992 *Phys. Rev.* A **46** 1886
Krech M and Dietrich S 1992 *Phys. Rev.* A **46** 1922
[46] Bastiaansen P J M and Knops H J F 1998 *Phys. Rev.* E **57** 3784
[47] Krech M 1999 *APS Centennial Mtg (Atlanta, GA, March 1999)* talk
[48] Garcia R and Chan M H W 1999 *Phys. Rev. Lett.* **83** 1187
Garcia R 1999 *APS Centennial Mtg (Atlanta, GA, March 1999)* talk
[49] Cheng E and Cole M W 1988 *Phys. Rev.* B **38** 987
[50] Mukhopadhyay A and Law B M 1999 *Phys. Rev. Lett.* **83** 772
Law B M 1999 *APS Centennial Mtg (Atlanta, GA, March 1999)* talk
[51] Musevic I, Slak G and Blinc R 1996 *Rev. Sci. Instrum.* **67** 2554
Musevic I, Slak G and Blinc R 1996 *16th Int. Liquid Crystal Conf. (Kent, OH)* abstracts, p 91
[52] Vilfan M, Musevic I and Copic M 1998 *Europhys. Lett.* **43** 41